



CHORUS

This is the accepted manuscript made available via CHORUS. The article has been published as:

Bound muon decay spectrum in the leading logarithmic accuracy

Robert Szafron and Andrzej Czarnecki

Phys. Rev. D **94**, 051301 — Published 6 September 2016

DOI: [10.1103/PhysRevD.94.051301](https://doi.org/10.1103/PhysRevD.94.051301)

Bound muon decay spectrum in the leading logarithmic accuracy

Robert Szafron^{1,*} and Andrzej Czarnecki¹

¹*Department of Physics, University of Alberta, Edmonton, Alberta, Canada T6G 2G7*

We compute the dominant, logarithmically enhanced radiative corrections to the electron spectrum in the bound muon decay in the whole experimentally interesting range. The corrected spectrum fits well the TWIST results. The remaining theoretical error, dominated by the nuclear charge distribution, can be reduced in the muon-electron conversion searches by measuring the spectrum slightly below the New Physics signal window.

I. INTRODUCTION

The spectrum of electrons from the decay of a muon bound in an atom (decay in orbit, DIO) has two parts. The low-energy part, $E_e \lesssim m_\mu/2$ (E_e is the electron energy and m_μ is the muon mass) is present also in the free muon decay but is reshuffled because the bound muon is moving and the daughter electron interacts with the electric field of the nucleus. This modification of the spectrum was observed by TWIST [1].

In addition, the possibility of transferring momentum to the nucleus approximately doubles the range of energy accessible to the electron, adding the high-energy region $m_\mu/2 \lesssim E_e \lesssim m_\mu$. This region has already been explored for some nuclei including titanium, sulfur and gold [2–6]. Upcoming experiments COMET and Mu2e [7–9] will measure it for aluminum with a high precision. Their main goal is to discover the lepton-flavor violating muon-electron conversion. High-energy electrons from the DIO are a background in this search.

The purpose of this paper is to improve the theoretical description of the entire spectrum by determining logarithmically enhanced radiative corrections. We focus on aluminum, the stopping material in COMET and Mu2e.

The spectrum of the free muon decay is known including corrections of the first [10] and of the second order [11] in the fine structure constant $\alpha \approx 1/137$, as well as the leading logarithms in the third order $\left(\frac{\alpha}{\pi} \ln \frac{m_\mu}{m_e}\right)^3$ [12]. In the case of the bound muon, even $\mathcal{O}(\alpha)$ effects are known only in a limited range of electron energies. Radiative corrections near the top of the electron spectrum in the free muon decay ($E_e \sim \frac{m_\mu}{2}$) were evaluated in [13] by convoluting the $\mathcal{O}(\alpha)$ free-muon spectrum with the so-called shape function [14], reconciling TWIST results [1] with quantum electrodynamics. This approach had been developed in the heavy quark effective theory to describe decays of B -mesons [15, 16] using factorization theorems. Alas, the factorization cannot be applied when the electron energy is much larger than the half of the muon mass.

Fortunately, the highest energy endpoint of the DIO spectrum ($E_e \sim m_\mu$) offers a different simplification: one

can expand in the number of photons exchanged with the nucleus, parameterized by $Z\alpha$ where Z is the proton number of the nucleus (for aluminum, $Z = 13$). Radiative corrections in the endpoint region have been evaluated in [17]. It is still unknown how to compute full radiative corrections for intermediate electron energies $\frac{1}{2}m_\mu < E_e < m_\mu$ [18].

However, the likely largest corrections can be computed. Enhanced effects $\sim \frac{\alpha}{\pi} \ln \frac{m_\mu}{m_e}$ arise from collinear photons and can be found from collinear factorization theorems [19], without a new loop calculation.

In a muonic atom, vacuum polarization (VP) is an additional source of large logarithms. It modifies the Coulomb potential and is taken into account numerically together with the effects of the finite charge distribution in the nucleus. Typically, the VP correction is on the order of $\frac{\alpha}{\pi} \ln \frac{Z\alpha m_\mu}{m_e}$, or $\frac{\alpha}{\pi} \ln \frac{m_\mu}{m_e}$ near the DIO endpoint.

Section II presents details of both collinear and VP corrections. Section III summarizes numerical results. In Section IV we discuss the uncertainty due to the nuclear charge distribution and suggest a means of lowering it.

II. LEADING LOGARITHMIC CORRECTIONS TO THE DIO SPECTRUM

We assume that the daughter electron is relativistic. For a low-energy electron, additional non-perturbative phenomena would have to be considered. For example, a slow electron can be captured into the atom in the final state. The low-energy part of the spectrum is not yet fully understood [20]. However, it involves only a small fraction of electrons because of the phase space suppression and it is not relevant for conversion experiments, sensitive only to the high-energy region of the spectrum.

A. Collinear photons

Focusing on an energetic electron, we first consider the emission of collinear photons. For electron energies much larger than the electron mass $E_e \gg m_e$, Coulomb corrections are small and do not affect the collinear limit of the amplitude in the leading order in $Z\alpha$. Before the emission of a collinear photon, the electron is almost on-shell and propagates over distances large compared with the size of the muonic atom. Hence, the collinear emission

* szafron@ualberta.ca

is a long-distance phenomenon that takes place after the electron escapes the region of the strong binding potential. On the other hand, if the photon is emitted before the last scattering of an electron on the nucleus, the electron is still off-shell and the amplitude is not singular. In such case, the corrections are not enhanced by a large logarithm $\ln \frac{m_\mu}{m_e}$ or are suppressed by additional powers of $Z\alpha$. For aluminum, $Z\alpha \ln \frac{m_\mu}{m_e} \sim \frac{1}{2}$. These corrections are comparable with the non-logarithmic term $\mathcal{O}(\alpha)$ and we neglect them.

Collinear corrections can be calculated using a factorization theorem, previously employed to improve the free muon spectrum [12, 21, 22]. Following Ref. [21] we evaluate the collinear logarithms $\frac{d\Gamma_{\text{CL}}}{dE_e}$ convoluting the leading order spectrum $\frac{d\Gamma_{\text{LO}}}{dE_e}$ with the electron structure function,

$$\frac{d\Gamma_{\text{CL}}}{dE_e} = \frac{d\Gamma_{\text{LO}}}{dE_e} \otimes D_e + \mathcal{O}\left(Z\alpha \frac{\alpha}{\pi} \ln \frac{m_\mu}{m_e}\right), \quad (1)$$

where

$$D_e(x) = \delta(1-x) + \frac{\alpha}{2\pi} \left(\ln \frac{m_\mu^2}{m_e^2} - 1 \right) P_e(x) + \mathcal{O}(\alpha^2) \quad (2)$$

The VP potential for an arbitrary charge distribution is given in Ref. [26]. The electron loop modifies the potential at distances comparable to the Compton wavelength of electron $r_e \sim \frac{1}{m_e}$ or smaller. The VP term reduces the endpoint energy and increases the number of high-energy electrons. It also shrinks the muon orbit. As a result, the muon kinetic energy and the lifetime increase.

In muonic atoms, the VP effect is much larger than in ordinary atoms [27]. The binding energy,

$$E_b \simeq -m_\mu \frac{(Z\alpha)^2}{2}, \quad (4)$$

receives a correction that is not suppressed by extra powers of $Z\alpha$. In an ordinary atom the Lamb shift contributes at the $(Z\alpha)^4$ order. For example, the VP correction starts with $-\frac{4}{15} \frac{\alpha}{\pi} (Z\alpha)^4 m_e$. This behaviour follows from the range of the VP potential, much smaller than the size of the electron orbit $\frac{1}{m_e} \ll \frac{1}{m_e Z\alpha}$. When the electron is replaced by a muon, the potential reaches beyond the muon orbit, $\frac{1}{m_e} \gg \frac{1}{m_\mu Z\alpha}$, and the correction to the binding energy behaves as $\sim \frac{\alpha}{\pi} (Z\alpha)^2 \ln \frac{m_\mu Z\alpha}{m_e}$. For a pointlike nucleus and using non-relativistic muon wave function, in the limit $m_e \ll m_\mu$, we get the correction to

and the electron splitting function is

$$P_e(x) = \left[\frac{1+x^2}{1-x} \right]_+.$$

We employ the dimensionless variable $x = E_e/E_{\text{max}}$ with E_{max} denoting the maximum electron energy. The convolution is defined as $A \otimes B(z) = \int_0^1 dx \int_0^1 dy \delta(z-xy) A(x)B(y)$ and the leading order term $\frac{d\Gamma_{\text{LO}}}{dE_e}$ includes Coulomb effects to all orders in $Z\alpha$.

Eq. (1) ensures a cancellation of the mass singularity in the correction to the bound muon lifetime, in agreement with the Kinoshita-Lee-Nauenberg theorem [23, 24].

B. Vacuum polarization

The second type of large logarithms comes from the vacuum polarization that strengthens the binding. The VP does not contribute to the free muon spectrum at one loop, hence this correction is exclusive to the bound muon and related to other binding effects. The $\mathcal{O}(\alpha)$ correction to the potential is known as the Uehling term [25]. For a pointlike nucleus the binding potential is

$$V(r) = -\frac{Z\alpha}{r} \left(1 + \frac{2\alpha}{3\pi} \int_1^\infty dx e^{-2m_e r x} \frac{2x^2 + 1}{2x^4} \sqrt{x^2 - 1} \right) + \mathcal{O}\left((Z\alpha)^3\right). \quad (3)$$

the binding energy

$$\Delta B_{\text{VP}} = \frac{\alpha}{\pi} (Z\alpha)^2 m_\mu \left(\frac{11}{9} - \frac{2}{3} \ln \frac{2m_\mu Z\alpha}{m_e} \right) = -2.7 \text{ keV for aluminum.} \quad (5)$$

This is larger than the total uncertainty in the binding energy and has to be included in the evaluation of the endpoint energy. We will return to this correction in the discussion of numerical results in Section III.

The logarithmic terms in the VP correction can also be reproduced by using in eq. (4) the running coupling constant $\alpha(Q^2) = \frac{\alpha}{1 - \frac{\alpha}{3\pi} \ln\left(\frac{Q^2}{m_e^2}\right)}$, with $\sqrt{Q^2} = m_\mu Z\alpha$.

In the DIO spectrum, the VP effects do not factorize, unlike the collinear corrections. They are accounted for, together with the finite nuclear size, by numerically solving the Dirac equation.

Large corrections with logarithms of $Z\alpha$ are also present in the DIO spectrum. Pure relativistic corrections can contain $\ln Z\alpha$, typically suppressed by two powers of $Z\alpha$ [28]. In our numerical approach, we solve the Dirac equation without any non-relativistic expansion; hence, these terms are automatically included in our leading order spectrum.

Logarithms of $Z\alpha$ will appear also in radiative corrections involving ultra-soft photons, like in the classical

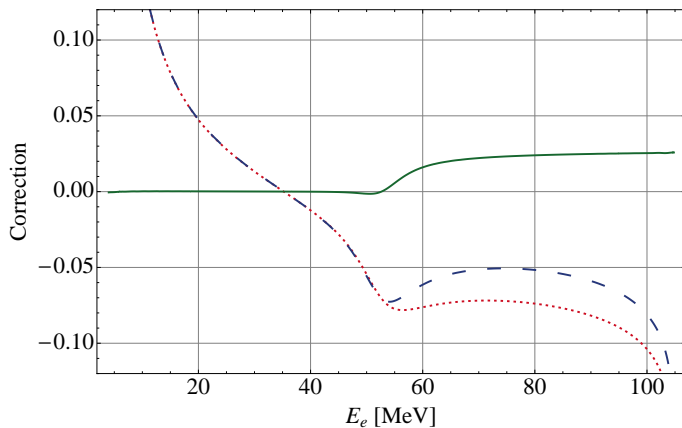


FIG. 1. Leading corrections to the bound muon spectrum. The VP correction $\frac{N_{VP}-N_{LO}}{N_{LO}}$ is mostly positive (solid line). We have shifted the electron energies in the VP term, $E_e \rightarrow E_e + \Delta B_{VP}$, so that the N_{VP} and N_{LO} spectra have a common endpoint energy, $E_{\mu e}$. The correction $\frac{N_{CL}-N_{LO}}{N_{LO}}$, due to collinear photons, decreases the number of electrons near the endpoint (dotted line). The dashed line represents the total correction. See text for details.

calculation of the Lamb shift [29]. These Bethe-type logarithms are suppressed by additional powers of $Z\alpha$, in the same manner as the VP shift of the binding energy in electron atoms.

III. NUMERICAL RESULTS

We compute wave functions of the bound muon and of the daughter electron by numerically solving the Dirac equation [30, 31]. An analytical solution is not known for a realistic distribution of the nuclear charge density. In order to find the DIO spectrum we have implemented in Python matrix elements, including nuclear recoil corrections, given in [32]. As a check of the numerical code, we have compared the muon binding energy and the DIO spectrum with previous results [32, 33].

We use the Fermi model for the nuclear charge density distribution fitted to the electron elastic scattering data [34]. In Section IV we discuss other possible models and the uncertainty related to the nuclear charge radius.

Near the endpoint, the spectrum rapidly varies with energy, like $(E_{\max} - E_e)^5$, so a precise value of E_{\max} is critical. We predict, including the charge distribution corrections, the VP term, and the recoil correction (see eq. (13) in [32]),

$$E_{\max} = m_{\mu} - E_{\text{rec}} + E_b = 104.971(1) \text{ MeV}. \quad (6)$$

The error comes from the uncertainty in the charge distribution. The difference between our result and the endpoint energy without the VP correction, $E_{\mu e} = 104.973(1)$ [32], is consistent with Eq. (5).

We denote $N_{CL} = \frac{d\Gamma_{CL}}{dE_e}$ and $N_{LO} = \frac{d\Gamma_{LO}}{dE_e}$. We also introduce $N_{VP} = \frac{d\Gamma_{VP}}{dE_e}$ as the leading order spectrum

that includes the VP correction only. Relative collinear $\frac{N_{CL}-N_{LO}}{N_{LO}}$ and VP $\frac{N_{VP}-N_{LO}}{N_{LO}}$ corrections are presented in Fig. 1. For a 1 MeV signal window near the endpoint, we obtain a 12% reduction of the number of DIO events, consistent with [17].

Should the DIO spectrum be needed for electron energies closer to the endpoint, we recommend using eq. (2) in [17], where soft photons have been exponentiated.

For low electron energies, $E_e \leq \frac{m_{\mu}}{2} - m_{\mu}Z\alpha$, the DIO spectrum is dominated by the free muon decay corrected by the binding effects. Consequently, in this region, the VP is a relatively unimportant subleading effect. The VP correction becomes significant for electron energies above the free muon endpoint, $E_e > \frac{m_{\mu}}{2}$, where the free muon spectrum is absent. Here, the spectrum is dominated by the binding effects and is sensitive to the details of the binding potential. The VP correction is particularly important near the endpoint $E_e \simeq E_{\max}$ where highly-virtual Coulomb photons transfer a large momentum to the nucleus.

In Fig. 2 we show the VP correction in the DIO endpoint region, where the spectrum has a simple dependence on the electron energy,

$$\frac{d\Gamma}{dE_e} \equiv N \sim (E_{\max} - E_e)^5. \quad (7)$$

Here the VP correction manifests itself in two ways. The correction due to the shift in the endpoint energy (5) is important only very close to E_{\max} . For smaller electron energies it becomes negligible. To illustrate this effect we plotted $\left(\frac{E_{\max}-E_e}{E_{\mu e}-E_e}\right)^5 - 1$ in Fig. 2.

The VP also modifies muon and electron wave functions. This effect does not depend strongly on the electron energy, because it is dominated by the running of the coupling constant $\alpha(Q^2)$. It varies slowly for $|Q^2| \sim m_{\mu}^2$.

To quantify this effect, we define the shift of the spectrum due to the VP correction to the wave functions as

$$\delta_{VP} = \frac{N_{VP}(E_e + \Delta B_{VP}) - N_{LO}(E_e)}{N_{LO}(E_e)} \quad (8)$$

in the limit when E_e approaches the endpoint of the leading order spectrum $E_{\mu e}$. We find numerically $\delta_{VP} = 2.5\%$. Ref. [17] provided the correction to the leading term of the spectrum expanded in $Z\alpha$: $\delta_{VP,(Z\alpha)^5} = 2.9\%$. The difference with δ_{VP} is caused by higher orders in $Z\alpha$, estimated as minus 20% of the leading $(Z\alpha)^5$ term [17].

As a check, we have compared our results with the spectrum measured by TWIST [1]. The results are presented in Fig. 3. The quality of the fit is comparable to our previous approach based on the shape function (see Fig. 3 in [13]). However, now we are not limited to electron energies $E_e \lesssim \frac{m_{\mu}}{2}$. Also, we are not including the energy scale uncertainty in the fit. This reduces the number of fit parameters to one: the overall normalization of the spectrum. The quality of the fit is characterized by χ^2 per degree of freedom, χ^2/dof . The leading order DIO spectrum gives $\chi^2/\text{dof}=8.8$. When radiative corrections

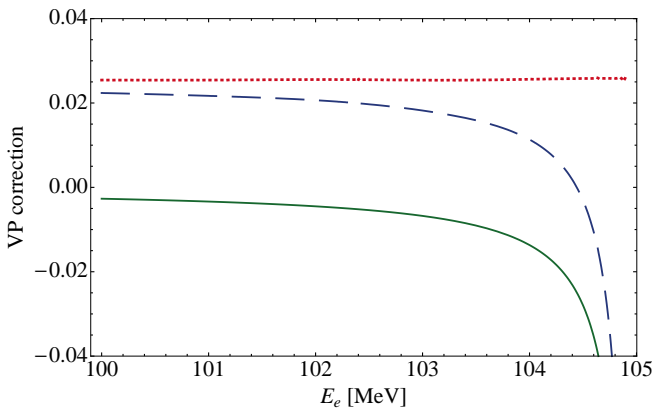


FIG. 2. Vacuum polarization correction to the DIO spectrum around the endpoint. The solid line illustrates the relative change of the spectrum due to the decrease of the endpoint energy, $\left(\frac{E_{\max}-E_e}{E_{\mu e}-E_e}\right)^5 - 1$. The dotted line is a correction due to the shift in the wave functions δ_{VP} , see Eq. (8). The dashed line shows both effects combined.

are included using the shape function, this decreases to $\chi^2/\text{dof}=3.9$. The spectrum obtained in the present paper gives a slightly better $\chi^2/\text{dof}=2.8$. The quality of the fit could likely be improved by including the TWIST systematic errors and correlations among energy bins but we are not qualified to do this.

IV. NUCLEAR CHARGE DISTRIBUTION

In order to quantify the uncertainty due to the nuclear charge density, we have examined three experimental sources. Two use the Fermi model,

$$\varrho(r) = \frac{\varrho_0}{1 + \exp\left(\frac{r-r_0}{a}\right)}, \quad (9)$$

where r_0 is a fitted parameter describing the radius of the distribution and a is related to the so-called skin thickness. Elastic electron scattering gives [34] $r_0 = 2.84(5)$ fm for $a = 0.569$ fm and transitions in muonic aluminum [35] give, more precisely, $r_0 = 3.0534(13)$ fm for $a = 0.523$ fm. Even though the radii seem to differ by more than one standard deviation, they have been fitted at different values of the parameter a . In our calculation these differences partially compensate one another, as we shall see below.

Another parameterization employs the spherical Bessel function j_0 ,

$$\varrho(r) = \sum_n a_n j_0\left(\frac{n\pi r}{R}\right), \quad r < R; \quad \varrho(r) = 0, \quad r \geq R, \quad (10)$$

where R is a cutoff beyond which the density is assumed to be zero, taken to be $R = 7$ fm, and the coefficients a_i , for $i = 1, \dots, 12$, are given in [34]. Unfortunately, no error estimate seems to be available for a_i .

Only the high-energy part of the DIO spectrum is sensitive to the smearing of the nuclear charge. Fig. 4 shows the predictions of the three models in that region, consistent within the electron scattering errors.

Electron scattering data give the largest error for the charge density. We use them to tabulate the DIO spectrum for aluminum including leading logarithmic corrections; see supplemental material [36]. This choice is further justified by the muon DIO amplitude near the endpoint being proportional to the elastic scattering amplitude [17]. To quantify the dependence of the error on the electron energy, we approximate the one-sigma boundaries (the shaded region in Fig. 4) by

$$\frac{\Delta N}{N} \approx \sigma \frac{2E_e - E_{\max}}{E_{\max}}, \quad \text{with } \sigma = 0.022. \quad (11)$$

The coefficient 2 in front of E_e reflects the approximate vanishing of the sensitivity to the nuclear distribution in the low-energy region: at $E_e = E_{\max}/2$ and below.

The uncertainty (11) can be reduced by measuring, in conversion experiments, the DIO spectrum outside the conversion signal window. To fit r_0 , such measurements should use the radiatively corrected DIO spectrum; not only are the corrections large but they also change the simple functional form of the DIO spectrum near the endpoint, Eq. (7).

To achieve the necessary accuracy, the DIO spectrum measurement requires a precise energy calibration. The endpoint energy has been calculated with a precision of 1 keV, see Eq. (6). The upcoming experiments will measure the endpoint energy with a larger uncertainty, ΔE_{\max} . From Eq. (7) we estimate how ΔE_{\max} influences the number of electrons with energy $E_e = E_{\max} - \delta$. Denoting the uncertainty in the spectrum due to ΔE_{\max} as ΔN_E we get

$$\frac{\Delta N_E}{N} \approx 5 \frac{\Delta E_{\max}}{\delta}, \quad (12)$$

hence in order to constrain the error related to the nuclear charge distribution, the number of DIO events N with energy E_e has to be measured with an experimental precision ΔN_{exp} such that

$$\sqrt{\left(\frac{\Delta N_{\text{exp}}}{N}\right)^2 + \left(\frac{\Delta N_E}{N}\right)^2} \lesssim \frac{\Delta N}{N} \quad (13)$$

It is most efficient to use the DIO measurement at an energy for which the largest $\frac{\Delta N_{\text{exp}}}{N}$ can be tolerated. This optimal energy can be calculated using (11) and (12),

$$\begin{aligned} \frac{E_e^{\text{opt}}}{E_{\max}} &= 1 - \xi - \frac{2}{3}\xi^2 - \frac{4}{3}\xi^3 + \mathcal{O}(\xi^4) \\ \xi &\equiv \sqrt[3]{\frac{25}{2} \left(\frac{\Delta E_{\max}}{\sigma E_{\max}}\right)^2} \end{aligned} \quad (14)$$

For example, for $\Delta E_{\max} = 30$ keV, the optimal energy is 90 MeV, and the experimental uncertainty should be smaller than $\frac{\Delta N_{\text{exp}}}{N} \lesssim 0.012$.

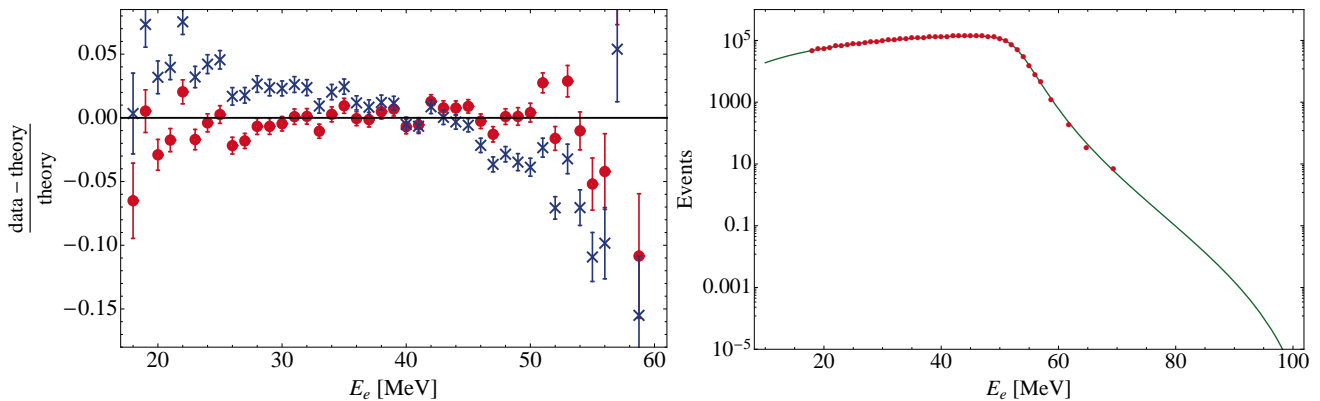


FIG. 3. Left panel: the difference between TWIST data and the theoretically calculated spectrum normalized to our theoretical evaluation of the DIO spectrum. Crosses represent the leading order evaluation without any radiative corrections. Dots correspond to our new evaluation that includes leading logarithmic corrections. Right panel: the DIO spectrum (solid line) fitted to TWIST data (dots). With the results of this paper, a measurement of the DIO spectrum at energies $E_e \sim \frac{m_\mu}{2}$ can be used to calibrate the energy response in the future conversion experiments.

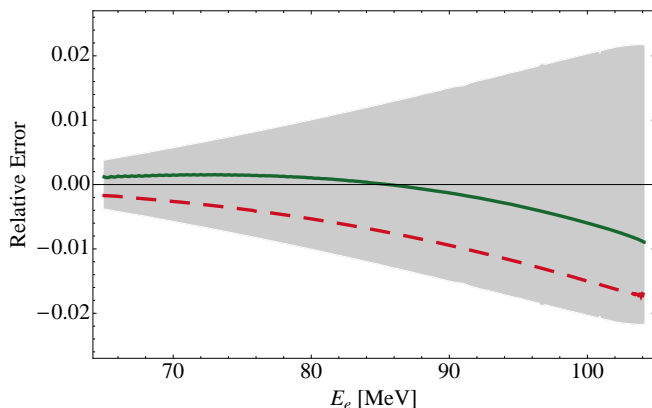


FIG. 4. Relative uncertainty in the DIO spectrum near the endpoint related to nuclear charge distribution. The shaded region is obtained by varying r_0 in (9) within limits obtained from electron scattering data [34]. Solid line corresponds to the Bessel parametrization (10) and the dashed line to the Fermi distribution obtained from muonic atoms [35].

V. CONCLUSIONS

We have calculated the energy spectrum of electrons in the bound muon decay including leading logarithmic corrections. For electron energies $E_e > 100$ MeV the sum of vacuum polarization and collinear photon effects decreases the number of DIO events by more than 10%,

in agreement with the endpoint expansion [17].

Our present result is valid in the entire energy range $E_e \gg m_e$ and can be used to calibrate the energy in conversion experiments. This was not possible with previous results available only near the endpoint E_{max} and in the low-energy (shape function) region, without means to interpolate in the remaining high-energy region.

The dominant remaining uncertainty comes from the nuclear charge distribution. Here new input from experiments is required. We suggest that the DIO spectrum be used to constrain the charge distribution, as a byproduct of the conversion search.

We have neglected the screening by the electron cloud (see [32] for a discussion). In order to further improve the theoretical description of the DIO spectrum, this effect should be included together with non-logarithmic radiative corrections $\mathcal{O}(\frac{\alpha}{\pi})$.

ACKNOWLEDGMENTS

This research was supported by Natural Sciences and Engineering Research Council (NSERC) of Canada. R.S. acknowledges support by the Fermilab Intensity Frontier Fellowship. Fermilab is operated by Fermi Research Alliance, LLC under Contract No. De-AC02-07CH11359 with the United States Department of Energy.

-
- [1] A. Grossheim et al. Decay of negative muons bound in Al-27. *Phys.Rev.*, D80:052012, 2009.
 [2] W. H. Bertl et al. A Search for muon to electron conversion in muonic gold. *Eur. Phys. J.*, C47:337–346, 2006.
 [3] C. Dohmen et al. Test of lepton flavor conservation in $\mu \rightarrow e$ conversion on titanium. *Phys. Lett.*, B317:631–636,

1993.
 [4] S. Ahmad et al. Search for Muon - Electron and Muon - Positron Conversion. *Phys. Rev.*, D38:2102, 1988.
 [5] R. A. Burnham et al. Search for μe Conversion in Ti. *Phys. Rev. Lett.*, 59:970–973, 1987.
 [6] A. Badertscher et al. A Search for Muon - Electron

- and Muon - Positron Conversion in Sulfur. *Nucl. Phys.*, A377:406–440, 1982.
- [7] L. Bartoszek et al. Mu2e Technical Design Report . 2014.
- [8] Y. G. Cui et al. Conceptual design report for experimental search for lepton flavor violating $\mu^- - e^-$ conversion at sensitivity of 10^{-16} with a slow-extracted bunched proton beam (COMET). 2009.
- [9] Y. Kuno. A search for muon-to-electron conversion at J-PARC: The COMET experiment. *PTEP*, 2013:022C01, 2013.
- [10] R. E. Behrends, R. J. Finkelstein, and A. Sirlin. Radiative corrections to decay processes. *Phys. Rev.*, 101:866–873, 1956.
- [11] C. Anastasiou, K. Melnikov, and F. Petriello. The Electron energy spectrum in muon decay through $\mathcal{O}(\alpha^2)$. *JHEP*, 09:014, 2007.
- [12] A. Arbuzov. Higher order QED corrections to muon decay spectrum. *JHEP*, 0303:063, 2003.
- [13] A. Czarnecki, M. Dowling, X. Garcia i Tormo, W. J. Marciano, and R. Szafron. Michel decay spectrum for a muon bound to a nucleus. *Phys.Rev.*, D90(9):093002, 2014.
- [14] R. Szafron and A. Czarnecki. Shape function in QED and bound muon decays. *Phys.Rev.*, D92(5):053004, 2015.
- [15] M. Neubert. QCD based interpretation of the lepton spectrum in inclusive $B \rightarrow X(u)l\bar{\nu}$ decays. *Phys.Rev.*, D49:3392–3398, 1994.
- [16] I. Y. Bigi, M. A. Shifman, N. G. Uraltsev, and A. I. Vainshtein. On the motion of heavy quarks inside hadrons: Universal distributions and inclusive decays. *Int.J.Mod.Phys.*, A9:2467–2504, 1994.
- [17] R. Szafron and A. Czarnecki. High-energy electrons from the muon decay in orbit: radiative corrections. *Phys.Lett.*, B753:61–64, 2016. arXiv:1505.05237.
- [18] R. Szafron. Bound Muon Decay. *Acta Phys.Polon.*, B46(11):2279, 2015.
- [19] R. Keith Ellis, W. James Stirling, and B. R. Webber. QCD and collider physics. *Camb. Monogr. Part. Phys. Nucl. Phys. Cosmol.*, pages 1–435, 1996.
- [20] C. Greub, D. Wyler, S.J. Brodsky, and C.T. Munger. Atomic alchemy. *Phys.Rev.*, D52:4028–4037, 1995.
- [21] A. Arbuzov, A. Czarnecki, and A. Gaponenko. Muon decay spectrum: Leading logarithmic approximation. *Phys.Rev.*, D65:113006, 2002.
- [22] A. Arbuzov and K. Melnikov. $\mathcal{O}\left(\alpha^2 \ln \frac{m_\mu}{m_e}\right)$ corrections to electron energy spectrum in muon decay. *Phys.Rev.*, D66:093003, 2002.
- [23] T. Kinoshita. Mass singularities of feynman amplitudes. *J. Math. Phys.*, 3:650–677, 1962.
- [24] T. D. Lee and M. Nauenberg. Degenerate Systems and Mass Singularities. *Phys. Rev.*, 133:B1549–B1562, 1964. [25(1964)].
- [25] E. A. Uehling. Polarization effects in the positron theory. *Phys. Rev.*, 48:55–63, 1935.
- [26] D. J. Hylton. Finite-nuclear-size corrections to the Uehling potential. *Phys. Rev.*, A32:1303–1309, 1985.
- [27] E. Borie and G. A. Rinker. The energy levels of muonic atoms. *Rev. Mod. Phys.*, 54:67–118, 1982.
- [28] R. Szafron. Rare Muon Decays. *Acta Phys.Polon.*, B44(11):2289–2294, 2013.
- [29] A. Pineda and J. Soto. The Lamb shift in dimensional regularization. *Phys. Lett.*, B420:391–396, 1998.
- [30] M. E. Rose. *Relativistic Electron Theory*. John Wiley and Sons, INC., New York, 1961.
- [31] H. Behrens and W. Bühring. *Electron radial wave functions and nuclear beta-decay*, volume 67. Oxford University Press, USA, 1982.
- [32] A. Czarnecki, X. Garcia i Tormo, and W. J. Marciano. Muon decay in orbit: spectrum of high-energy electrons. *Phys.Rev.*, D84:013006, 2011.
- [33] R. Watanabe, M. Fukui, H. Ohtsubo, and M. Morita. Angular Distribution of Electrons in Bound Muon Decay. *Prog. Theor. Phys.*, 78:114–122, 1987.
- [34] H. De Vries, C. W. De Jager, and C. De Vries. Nuclear charge-density-distribution parameters from elastic electron scattering. *Atomic data and nuclear data tables*, 36(3):495–536, 1987.
- [35] G. Fricke, J. Herberz, Th. Hennemann, G. Mallot, L. A. Schaller, L. Schellenberg, C. Piller, and R. Jacot-Guillarmod. Behavior of the nuclear charge radii systematics in the s-d shell from muonic atom measurements. *Phys. Rev.*, C45:80–89, 1992.
- [36] See Supplemental Material at [URL will be inserted by publisher] for a tabulated version of the DIO spectrum for aluminum.